AFAL-TR-87-096

AD:

(4)

Final Report
for the period
1 June 1985 to
31 March 1987

Advanced Electric Propulsion MPD

May 1988

Authors:
R. G. Jahn
A. J. Kelly
J. Polk

Princeton University
Dept of Mechanical & Aeronautical Engineering
School of Engineering/Applied Science
Princeton, NJ 08544

MAE 1791
F04611-85-C-002

Approved for Public Release

Prepared for the:

Air Force Astronautics Laboratory

Air Force Space Technology Center
Space Division, Air Force Systems Command
Edwards Air Force Base,
California 93523-5000

SECURITY CLASSIFICATION OF THIS PAGE

REPORT DOCUMENTATION PAGE

Form Approved OMB No. 0704-0188

1a REPORT SECURITY CLASSIFICATION: UNCLASSIFIED	1b RESTRICTIVE MARKINGS
2a SECURITY CLASSIFICATION AUTHORITY	3 DISTRIBUTION/AVAILABILITY OF REPORT: Approved for public release; distribution is unlimited.
2b DECLASSIFICATION/DOWNGRADING SCHEDULE	
4 PERFORMING ORGANIZATION REPORT NUMBER(S): MAE 1731	5 MONITORING ORGANIZATION REPORT NUMBER(S): AFAL-TR-87-096
6a NAME OF PERFORMING ORGANIZATION: Princeton University; 6b OFFICE SYMBOL (If applicable):	7a NAME OF MONITORING ORGANIZATION: Air Force Astronautics Laboratory
6c ADDRESS (City, State, and ZIP Code): Department of Mechanical & Aeronautical Eng. School of Engineering/Applied Science Princeton, NJ 08544	7b ADDRESS (City, State, and ZIP Code): LSVE Edwards AFB CA 93523-5000
8a NAME OF FUNDING/SPONSORING ORGANIZATION; 8b OFFICE SYMBOL (If applicable):	9 PROCUREMENT INSTRUMENT IDENTIFICATION NUMBER: F04611-85-C-0021
8c ADDRESS (City, State, and ZIP Code)	10 SOURCE OF FUNDING NUMBERS: PROGRAM ELEMENT NO. 62302F; PROJECT NO. 5730; TASK NO 00; WORK UNIT ACCESSION NO HU

11 TITLE (Include Security Classification)

Advanced Electric Propulsion MPD (U)

12 PERSONAL AUTHOR(S)

Jahn, R. G., Kelly, A. J., and Polk, J.

13a TYPE OF REPORT	13b TIME COVERED	14 DATE OF REPORT (Year, Month, Day)	15 PAGE COUNT
Final	FROM 85/6/1 TO 87/3/31	88/5	39

16 SUPPLEMENTARY NOTATION

17 COSATI CODES			18 SUBJECT TERMS (Continue on reverse if necessary and identify by block number)
FIELD	GROUP	SUB-GROUP	Magnetoplasmadynamic Thruster, Cathode Erosion, Surface Layer Activation, Radioactive Tracer, Nuclear Activation.
21	03		

19 ABSTRACT (Continue on reverse if necessary and identify by block number)

Magnetoplasmadynamic (MPD) thrusters are inherently low thrust devices, consequently operation for hundreds to thousands of hours will be required to impart useful levels of total impulse. Experience at Princeton and in other laboratories indicates that the cathode of these devices suffers the most severe damage in the hostile environment of the high current discharge, therefore representing the life-limiting component. To explore the physical mechanisms responsible for cathode degradation, a new diagnostic tool has been developed - the surface layer activation (SLA) technique - to monitor erosive loss. This method was chosen in the Phase I portion of this contract from several alternatives because it provides highly accurate, in-situ measurements of erosive mass loss and can be readily applied to a wide variety of materials and environments. Concurrent programs of erosion measurement on experimental MPD thrusters using this technique and supporting analytical modelling of the erosion process are now being pursued.

The SLA diagnostic technique relies upon the production of a radioactive tracer in a thin

20 DISTRIBUTION/AVAILABILITY OF ABSTRACT	21 ABSTRACT SECURITY CLASSIFICATION
☒ UNCLASSIFIED/UNLIMITED ☐ SAME AS RPT ☐ DTIC USERS	UNCLASSIFIED
22a NAME OF RESPONSIBLE INDIVIDUAL: Terry M. Banks, 2LT, USAF	22b TELEPHONE (Include Area Code): (805) 275-5473; 22c OFFICE SYMBOL: LSVE

DD Form 1473, JUN 86 — Previous editions are obsolete. — SECURITY CLASSIFICATION OF THIS PAGE

Block 19 (continued): layer near the cathode surface by nuclear activation. Monitoring changes in the activity level during thruster operation provides a direct measure of the amount of the activated layer removed by the destructive plasma-surface interaction. Partial results of preliminary tests of the technique have already been reported. The purpose of this report is to provide the completed set of preliminary data, discuss substantial improvements which make surface layer activation a practical tool, and describe the current direction of the experimental program.

TABLE OF CONTENTS

LIST OF TABLES

LIST OF FIGURES

INTRODUCTION

Because magnetoplasmadynamic (MPD) thrusters are inherently low thrust devices, operation for hundreds to thousands of hours will be required to impart useful levels of total impulse. Experience at Princeton[1,2] and in other laboratories[3,4] indicates that the cathode of these devices suffers the most severe damage in the hostile environment of the high current discharge, therefore representing the life-limiting component. To explore the physical mechanisms responsible for cathode degradation, a new diagnostic tool has been developed, the surface layer activation (SLA) technique, to monitor erosive loss. This method was chosen in the Phase I portion of this contract from several alternatives because it provides highly accurate, in-situ measurements of erosive mass loss and can be readily applied to a wide variety of materials and environments. Concurrent programs of erosion measurement on experimental MPD thrusters using this technique and supporting analytical modelling of the erosion process are now being pursued.

The SLA diagnostic technique relies upon the production of a radioactive tracer in a thin layer near the cathode surface by nuclear activation. Monitoring changes in the activity level during thruster operation provides a direct measure of the amount of the activated layer removed by the destructive plasma-surface interaction. Partial results of preliminary tests of the technique have already been reported[1]. The purpose of this paper is to provide the completed set of preliminary data, discuss substantial improvements which make surface layer activation a practical tool, and describe the current direction of the experimental program.

In the interests of clarity and conciseness, many details of the work have been omitted. A comprehensive archival literature base exists for this work in the form of monthly technical progress reports which are available from the Princeton University Engineering Library. The documents for this reporting period have been bound into yearly compendia which can be obtained by requesting MAE Report #1678 for 1985 and MAE Report #1679 for 1986. Alternatively, individual monthly reports relating to specific topics can be obtained directly from A.J. Kelly.

PRELIMINARY TESTS ON A HALF-SCALE FLARED ANODE THRUSTER

APPARATUS AND PROCEDURE

The coaxial thruster configuration shown in Figure 1 was chosen for the second test of the surface layer activation technique because preliminary performance data[5] indicated that this design is superior to the benchmark configuration studied in the first test. In this design, a high speed solenoid valve controls the injection of argon through the boron nitride backplate via an annulus surrounding the central 2% thoriated tungsten cathode and by 12 small holes arrayed on a circle near the copper anode. The thruster was mounted in a fiberglass vacuum tank 1.8 m in diameter and 4.8 m long, which was typically maintained at a pressure of about 10^{-5} torr. One msec duration rectangular current pulses were supplied by a 3000 μF, 175 kJ pulse-forming network.

The activation process will be discussed in detail in the next section; however, a brief description of the activation and data reduction used in this experiment is included here to demonstrate several deficiencies which have subsequently been corrected. Gamma emitting radionuclide tracers were produced by activating small spots 5 mm in diameter on the tungsten cathode, copper anode, and boron nitride backplate at the Princeton Cyclotron using the parameters listed in Table 1. These spots were placed at positions of maximum current density[5] where the most severe erosion presumably occurs. The resulting activity was monitored by observing prominent photopeaks in the gamma ray spectrum, which was collected with standard radiation detection equipment mounted outside the thruster. Gamma rays absorbed by a Bicron 5x5 inch NaI(Tl) scintillator crystal produce a number of photons proportional to the gamma energy. The photons are detected with a photomultiplier tube, which produces voltage pulses that are then read

and displayed as the number of detected decay events (counts) in a particular energy range (channel) by a Canberra Series 35 multichannel analyzer. The composite gamma ray spectrum of the lab background and the three isotopes produced in the activation is shown in Figure 2.

The activity of each source is proportional to the number of counts in the photopeak, which was determined by subtracting the background which is assumed to be linear and summing the remaining counts, as shown in Figure 3. To relate the fraction of the original activity remaining to the amount of material removed by erosion, the distribution of the radioactive tracer in the activated layer must be known. This was determined[6] by repetitively lapping thin layers from an irradiated sample of the material of interest and determining the remaining activity to produce a calibration curve such as that plotted in Figure 4.

The test sequence for this experiment consisted of 10,000 1 msec long discharges at an argon mass flow rate of 2.2 g/s and a current level of 9.6 kA (below the onset current), followed by 4000, 1 msec discharges at 0.75 g/s and 12 kA (above onset). The activities of the three isotopes were measured periodically during this sequence to determine the cumulative material losses.

RESULTS

No anode or backplate erosion was detected for either operating condition. The cumulative cathode mass loss per unit surface area is plotted in Figure 5 as a function of the number of discharges for both operating conditions. Figure 6 displays the same data plotted against the total charge transferred through the cathode; however, because the eroded mass is more likely a function of the local current density in the activated spot, which may have differed for the two operating conditions, comparisons of the two sets may not be valid. The most striking characteristic of the data is that regions of strongly linear behavior are separated by regions of discontinuous mass loss, a behavior not found in the first application of the technique[1,2]. As shown in the figures, the continuous regions are well represented by straight line fits which yield the erosion rates listed in Table 2, which are similar to weight loss measurements made at Stuttgart[7] and Tokyo[3].

Although no surface distortion in the activated spot was visible on a macroscopic or microscopic scale prior to the test, after the 14,000 discharges the spot was clearly visible as a shallow depression with a flat floor and a rim of tungsten that apparently melted and peeled away from the center. A similar blister was found on the cathode used in the first test of the technique. Inspection of the cathode surface under an optical microscope revealed a number of pits or craters which were densely packed and very distinct at the tip, less dense and distinguishable in the center and very indistinct at the base, where large scale surface melting and flowing had occurred. Under moderate magnification, small metallic spheres, apparently tungsten, were visible on the backplate near the annular injection port which surrounds the cathode.

Much smaller scale cratering was evident under a scanning electron microscope, typified by the photomicrograph in Figure 7. The typical crater diameter was 1 to 5 microns at the tip and the base, and 1-2 microns in the center. No qualitative differences or general differences in scale could be discerned on a microscopic level between the irradiated spot and regions surrounding it. One of the larger pits visible in the optical microscope was examined with the SEM, and appeared as a depression 60-70 microns in diameter thickly overlaid with the smaller craters. Sub-micron wide cracks in the surface were visible in all regions.

DISCUSSION

The appearance of the activated spot after the experiment strongly suggests that atypical surface damage occurred, probably due to material property changes induced by the high energy ion bombardment which produced the radioactive tracer. The fraction of tungsten transmuted to ^{185}Os was $O(10^{-12})$, so its presence as an impurity could not be responsible. A more likely explanation is that radiation damage from the 23 MeV α-particles used for the activation caused the

rupture of the surface during the experiment. Gross loss of material from the peeled back edges of the region may have been responsible for the discontinuous jumps in the erosion data. Concern that the measurement process is significantly disturbing the measured phenomenon motivated a critical examination of the activation process, which culminated in the definition of criteria governing the choice of an activation scheme capable of providing honest estimates of surface degradation. The results of that study are summarized in the next section.

The validity of the erosion rates obtained from the continuous portions of the data are defensible on the basis of the qualitative similarity between the microscopic erosion structures found in the activated spot and the undisturbed regions around it and the reasonable agreement with other measurements. Assuming similar erosion rates over the entire cathode yields an erosion rate of about 1 μg/C, or approximately 0.01 g/s at 10 kA, which is clearly unacceptably high for a practical device.

On cold cathode surfaces current continuity is maintained primarily through a number of small emission sites where the local temperature is extremely high, liberating electrons from the surface through a combination of thermal and field emission. The photomicrographs of the cathode surface confirm that the erosion processes occur primarily in localized microspots corresponding to the emission sites where temperatures exceed the melting temperature. The photomicrographs showing molten tungsten splashed from these sites and the tungsten droplets found on the backplate indicate that droplet erosion may be a significant component of the mass flux from the cathode surface, although the high local temperatures also imply high evaporation rates. The appearance of larger pits around 100 microns in diameter and the smaller craters 1-5 microns in diameter suggests that two types of arc attachment may occur. This is consistent with Rakhovskii's observations of a vacuum discharge using high speed photographic techniques[8]. He found two types of luminous spots--fast moving spots that left small craters and slower ones that tended to cluster and cause more extensive damage.

Evidence exists that when the bulk cathode surface temperature becomes sufficiently high, diffuse thermionic emission provides sufficient current and the local melting associated with the microspot mode of emission does not occur, allowing an erosion rate several orders of magnitude lower than that experienced with cold cathode bulk temperatures[7]. This provides some hope that steady state thrusters in which the cathode is heated by the discharge may have acceptable cathode lifetimes. The next stage of experimentation described in the final section of this paper is designed to explore this regime of cathode operation.

ANALYSIS OF THE SURFACE LAYER ACTIVATION TECHNIQUE

Two critical operations compose the the SLA mass loss measurement technique. First, a suitable gamma-emitting tracer must be produced in a thin surface layer; second, the change in activity of this source as it erodes must be determined. The activation and spectrum analysis fundamentals will be introduced next to establish the processes and terminology used subsequently in defining criteria for successful application of the technique. Finally, a new activation scheme will be presented which more satisfactorily meets these criteria than that used in the preliminary tests, and which is conceptually capable of providing a direct measure of the extent of surface pitting.

PRODUCTION OF THE RADIOACTIVE TRACER

The key to the SLA technique is the depth calibration curve, which relates the observable activity decline to the desired measurement of mass loss. As intimated earlier, this relationship is dependent on the distribution of the radionuclide beneath the surface. Because this technique relies on a nuclear reaction in the target surface excited by a high energy ion beam, the resulting distribution is dependent on the physics of that interaction. The density of the radioactive atoms n_a

is the number of target atoms that undergo the particular nuclear reaction during bombardment

$$n_a(x,y,z) = \int \sum_i n_{ti}(x,y,z)\ \sigma_i(E)\ \phi(x,y,z,t)\ dt$$

where n_{ti} is the density of isotope i in the target material, σ_i is the cross-section for reactions between the beam particle of energy E(x,y,z) and target isotope i, ϕ is the flux of beam particles, and t is the total irradiation time. The sum is taken over all reactions between the beam particle and isotopes in the target which produce the radioisotope. The x-, y-, and z-axes form an orthogonal coordinate system originating at the intersection of the beam and the target surface, with the z-axis directed into the target along the beam axis. Assuming isotropic target density, a constant ion energy across the beam, and an isotropic and time-independent beam density (no variation in the incident beam and negligible loss of particles by interactions along the path of interest in the target) yields

$$n_a(z) = \sum_i n_{ti}\, \sigma(E)\, \phi\, t \qquad (2)$$

ϕt represents the total dose, which can be measured during activation. Reaction cross-sections are often available from measurements or theoretical calculations; for instance, Figure 8 shows the cross-section for the $^{65}Cu(p,n)^{65}Zn$ reaction[9-11]. Since the cross-section is a function of the beam particle energy, the z-dependence of the energy in the target must be determined to calculate density profiles along z.

At energies above about 1 MeV, the incident particle loses energy primarily through interaction with the electrons of the target material. This energy loss can be reliably calculated to within about 1%[12-14]. The energy loss can be integrated along the actual particle path to obtain the energy, but the projection of the actual path onto the z-axis must be determined for our purpose. Fortunately, large angle scattering is rare in encounters with electrons at high energies, so above 1 MeV the path of the incident ion is very nearly straight[13]. Below 1 MeV, corrections for interactions with the target nuclei and for deviations from a straight path must be made. Since the nuclear reactions of interest have threshold energies above 1 MeV, however, this is unnecessary. Figure 9 displays the calculated proton energy in copper assuming the 4.51 MeV incident energy used in the copper activation. The extent of the activated layer is determined by the point in the target where the incident particle energy drops to the reaction threshold energy, as illustrated in Figure 9.

The density referenced to the η-axis normal to the surface and directed inward is simply related to that calculated above by the cosine of the polar angle θ between the beam axis and the surface normal:

$$n_a(\eta) = \sum_i n_{ti}\, \sigma_i(E)\, \phi\, t \,/\, \cos\theta \qquad (3)$$

with E expressed as a function of η.

The depth calibration curve relates the fractional activity remaining after removal of a certain amount of material. [illegible] the density of activated material is uniform in the activated layer, the relationship will depend on the [illegible]

$$\xi(p_i) = [illegible] \int [illegible]\ n_a(z)\, dz \qquad (4)$$

where $\xi(p_i)$ is the fractional activity remaining after [illegible] with ρ_t the target density and [illegible] z_t is the thickness of the activated layer. The simplest geometry to implement experimentally [illegible] the removal of [illegible] layers from the

activated area, which is in fact the process used to generate empirical depth calibration curves. This calibration relation is expressed theoretically as

$$\xi(\rho_t \eta' A) = \left(\int_0^{\eta'} n_a(\eta)\, d\eta \right) / \left(\int_0^{\eta_0} n_a(\eta)\, d\eta \right) \qquad (5)$$

where $\xi(\rho_t \eta' A)$ is the fractional activity remaining after a layer of thickness η' and area A has been removed and η_0 is the depth of the activated layer measured perpendicular to the surface. Of course, for data analysis the inverse relation is required. Figure 10 demonstrates the agreement between the measured depth calibration curves and the curve generated by integrating the calculated density for the copper activation. The close correspondence between the modelling and experiment indicates that the ultimate utility of theoretically generating depth calibration curves is limited only by the availability of appropriate cross-section data.

ANALYSIS OF THE RESULTING GAMMA SPECTRUM

Two methods of collecting and analyzing activity change data have been developed. The first relies on a comparison of the gamma spectrum after operation of the thruster with the initial spectrum, which yields the total activity change occurring during operation. This method is simple and highly accurate if the correct approach is used, as described next. The second method involves monitoring the countrate of a portion of the spectral region during operation, and while it is not as accurate, it allows real-time, time-resolved mass loss measurement.

The spectrum analysis method used in the preliminary tests relied on a linear approximation for the background spectrum, an assumption that is in general not justified, particularly when photopeaks overlap, as the ^{7}Be and ^{185}Os peaks do in Figure 2. Not the least worrisome aspect of this approximation is that the error cannot be estimated reliably. The following method is much more sound theoretically and has been tested and found to eliminate virtually all of the uncertainty in the activity measurement.

The assumptions underlying this method of spectrum resolution are[15]:

a) The sample spectrum is produced by a combination of known isotopes.
b) The response function of the detector for each isotope is known and is independent of the activity level.
c) The sample spectrum is a linear combination of the response functions of the component isotopes.
d) Each component has a different spectrum, all of which are linearly independent.

The first of these is easily met in this experiment, since the isotopes produced in the activation are known. The response function required in (b) can be determined by measuring the shape of the gamma spectrum of an isolated source with the same detector-source geometry to be used in the experiment, provided the count rate is low enough to avoid coincidence summing errors. (c) is also valid if the count rate is low enough, and can be expressed as

$$N_i = \sum_k x_k A_{ki} + \varepsilon_i \qquad (6)$$

where N_i is the number of counts in channel i, x_k is the intensity of radioisotope k relative to the measured response function (the fractional activity, if the response function is measured from the activated component prior to erosion), A_{kj} is the number of counts in channel i in the response function for isotope k, and ε_i is the measurement error. The background can be considered one of the source spectra or measured separately and subtracted out to produce pure source spectra. Assumption (d) must be met by a careful selection of isotopes.

A linear least squares program is used to obtain the best estimate of the intensities c_k.[1?] The error is inversely proportional to the number of counts in each channel, and can be reduced to an arbitrarily low value by increasing the counting time or averaging over a number of [illegible]. Errors less than 0.5% have been obtained routinely with microcurie level sources[15].

Instead of analyzing the photopeaks in the spectrum collected after operation of the th[illegible] which yields the time-integrated mass loss, the total counts in a particular energy range can be monitored as a function of time. The decrease in the counting rate with time is then a direct measure of the material lost during that time. The multichannel analyzer used in the convention[illegible] analysis method can be programmed to operate in this mode by initially setting upper and lower level discriminators to filter out all pulses outside a specified range and then displaying in successive channels the pulses counted during a certain dwell time. The pulse height range can be chosen to isolate the spectral region with the most intense photopeaks, which will maximize the signal-to-noise ratio, and the dwell time per channel can be varied from microseconds to hours to give an appropriate number of counts per channel and sufficient time resolution for the erosion process being studied. Preliminary estimates confirm that modest levels of activity should pr[illegible] data with a fairly low level of uncertainty for time resolution down to about 0.1 second.

CRITERIA FOR CHOICE OF AN ACTIVATION SCHEME

The following practical considerations govern the choice of activation schemes, wh[illegible] characterized by the beam energy and type, the shape and magnitude of the cross-section, the threshold energy for the reaction, the pr[illegible] of the reaction products, and the method [illegible] spectrum resolution, as explained above.

1. High Reaction Yield

The yield Y can be expressed as the number of radioisotope atoms produced per unit deposited beam material, and is governed by the energy of the beam and the magnitude of the cross-sections involved:

$$Y = \int \sum_i n_{ti}\, \sigma_i(E)\, dz$$

The same value can be expressed in more practical terms as the number of microcuries of a[illegible] produced per unit charge of beam ions deposited on the target with the conversion factor of (1.873 x 10[illegible] [illegible] where T[illegible] half life in seconds.

[illegible] to minimize damage to the [illegible]. Radiation damage is [illegible] defects created when atoms are displaced [illegible] particle with a primary knock-on target atom (pka). The [illegible] of these point defects recombine during the diffusion that occurs even at room temperature; however, some will cluster together to form extended defects such as dislocation loops and lines and cavities which are much more stable [illegible] microstructural changes caused by the formation of extended defects and the segregation of impurities or alloying materials which can accompany the condensation of point defects can result in macroscopic material property changes which are referred to as radiation effects. The number of point defects initially created by an [illegible] can be calculated [illegible] as described in the next few paragraphs. Because the formation of extended defects depends on the detailed kinetics of vacancy and interstitial migration and interaction with sinks, theoretical prediction of the resulting microstructural and microcompositional changes is much more difficult, so this extension of the analysis will not be pursued. It should be noted qualitatively, however, that the presence of the highly insoluble gas helium in the damaged lattice at concentrations as low as tens of ppm can significantly aggravate cavity formation and the resulting effects[19].

The number density of primary knock-ons can be calculated using the formula

$$n_{pka} = \phi\, t\, n_t\, \sigma_d \qquad (8)$$

which is similar to that used to calculate the density of activated atoms. Here n_t is the density of target atoms and σ_d is the cross-section for displacing lattice atoms. The cross-section for energy transfer greater than that required for displacement can be approximated for energies above a few keV using the Rutherford formula, which describes Coulomb interactions between the bombarding and target nuclei[20]. This equation is inversely proportional to incident particle energy, reflecting the fact that at high energies most of the energy loss is due to interaction with the target atom electrons, not the nuclei. This guarantees that most of the radiation damage will occur near the mean depth of penetration where the incident particle energy is lowest. The number density of displacements is found by multiplying the number of primary knock-ons by the average number of defects produced per pka, which is calculated by averaging over the Rutherford cross-section[21].

Figure 11 shows the damage profile in terms of the number of displacements per target atom (dpa) for 23 MeV alphas on tungsten at the dose used in the preliminary tests. As indicated above, the damage peaks near the mean depth of penetration. The damage is about 1 dpa for most of the path, but jumps to several hundred dpa near the end. In other words, each target atom is knocked from its lattice site several hundred times during the activation. Figure 12 shows the distribution of implanted He for the alpha activation, assuming a gaussian centered on the mean depth of penetration with the spread given by Ziegler[15], which is based on the range straggling calculations of reference 22. The He concentration reaches a peak of about 5% or 50,000 ppm at the mean depth of penetration.

Although the detailed kinetics have not been examined, it is not unreasonable to conclude that the problems encountered with the alpha activation were caused by the combination of a high concentration of implanted He coincident with the highly damaged region at the mean depth of penetration. The combination almost guarantees cavity formation, which was probably aggravated by the elevated temperatures encountered during operation. The cavities may have coalesced into a blister which ruptured, or the high density of smaller discrete cavities may have decreased the heat conduction into the cathode bulk enough to overheat and preferentially melt the 70 micron layer above it. The jumps seen in the preliminary mass loss data could have been caused by episodic loss of gross amounts of material in the molten layer.

For metals, it is recommended that the dose not exceed about 10^{16} cm^{-2} to avoid changes in the target properties[23]. This maximum allowable dose places a limit on the quantity of radioactive product generated per unit area. The reaction must therefore have a high enough yield to give a sufficient initial activity R within this limit:

$$R = C\, A\, Y\, (\phi\, t)_{max} \qquad (9)$$

where A is the surface area exposed to the beam.

The limit on allowable dose can be expressed as the area which must be irradiated at the maximum dose to give an acceptable level of activity. In other words, one can compensate for a low yield reaction by irradiating a larger area. This method of compensation obviously competes with the need to irradiate small areas to obtain spatially resolved data. For the cathode, high spatial resolution is only required in the axial direction if axisymmetry is assumed. Therefore, a circumferential zone can be irradiated instead of a spot to increase the area without sacrificing axial resolution. However, because of attenuation through the tungsten cathode only a certain fraction of the total activity can be observed perpendicular to the cathode axis. For a 1 cm diameter cathode this fraction is about 68%.

2. Adequate Reaction Cross-section Shape.

The depth of activation and the shape of the radioisotope density profile are dependent on the

beam energy and the shape of the cross-section curve at and below the beam energy. The following requirements form criteria that must be satisfied by proper choice of incident particle energy and reaction.

a. Activation Depth

The activated layer should be sufficiently deep that data can be collected for a reasonable period of operating time and so that the craters characteristic of arc damage do not puncture the layer. These considerations must be balanced against the required sensitivity of the technique. The fractional change in activity level is roughly the same as the fraction of the activated layer removed. Therefore, if it is possible to detect a 1% change in activity, for instance, then the sensitivity is limited to about 1% of the activated depth, and is inversely proportional the thickness of the layer.

b. Activation Profile

The density profile of the radioactive tracer is important because of its effect on the interpretation of the data. The measured depth calibration curves assume mass loss in the form of thin uniform layers. As explained above, a different depth calibration is required if the geometry of material loss differs from that assumed and significant biases can be introduced by using an inappropriate depth calibration. The ratio of the actual mass loss to that calculated using the thin slice depth calibration is

$$\beta(\eta_a) = \int_V dV \,/\, A\,\eta_a \qquad (10)$$

where η_a is the thickness of a slice giving an equivalent activity change:

$$\int_V n_a\, dV = A \int n_a(\eta)\, d\eta \qquad (11)$$

For instance, removing tungsten in small hemispherical craters rather than uniform slices from a cathode activated with 23 MeV α particles produces the bias plotted in Figure 13. Unfortunately, as the plot shows, the bias is a function of starting depth, surface damage scale, and surface damage geometry. For the largest crater diameter, the underestimation in mass loss occurs when the crater punches through the activated layer. For the smaller craters, the effect is due to the non-uniform distribution of the radioisotope. As equation (11) shows, if the radioisotope density were uniform, the volumes of the actual damage and the equivalent slice would be equal, rendering the data interpretation independent of geometry.

The allowable deviation from a uniform density profile depends on the desired accuracy and is difficult to define precisely, since the bias depends inherently on the expected geometry of material removal. Calculations can be performed to compare specific activation schemes, however. In addition, non-uniform erosion can be studied with an activation scheme which produces two radioisotopes with different depth distributions[20]. Comparison of the changes in activity of the two sources can reveal the scale of a particular geometry of mass loss, relaxing to some extent the requirement for profile uniformity and providing an ever more detailed picture of the erosion process.

3. Usable Reaction Products.

The radioisotopes produced by the reaction should meet these requirements.

a. Half-life.

The combined effect of natural decay and mass loss must not reduce the activity below detectible limits before the experiment is completed. This obviously depends on the initial activity, the half-life of the isotope, and the mass loss during the experiment. These parameters can be

examined in detail for a particular experiment and desired accuracy, keeping in mind that low activity levels can be somewhat compensated for by longer counting times, but it is a good rule of thumb not to plan an experiment lasting longer than three half-lives.

b. Spectral Separation.

For the least-squares method of spectrum analysis to resolve spectra with multiple sources, the response functions of those sources must be linearly independent. So, if several isotopes are produced in a single component, or if several activated components contribute to the spectrum, their individual spectra must be sufficiently different to allow precise resolution.

c. Measurable Response Functions.

Another requirement dictated by the least squares method is that it be possible to obtain single-source response functions, which is easily satisfied for activation schemes which yield only one gamma emitter. For those activations which produce more than one isotope, however, there must be some method of measuring the individual spectra. For isotopes with different half-lives or different depth profiles it may be possible to isolate one isotope by allowing the shorter lived ones to decay sufficiently or by lapping off those with shallower profiles. In addition, a number of pure sources are available commercially.

THE IMPROVED ACTIVATION PROCEDURE

Table 3 compares the tungsten activation scheme used in the preliminary tests with the deuteron activation chosen for subsequent experiments on the basis of the criteria given above. The results of the preliminary tests with the α-activation demonstrate the consequences of exceeding the dose limit for avoiding structural damage. The new deuteron activation produces several isotopes with a much larger yield, affording extremely good spatial resolution within the allowable dose limits. Figure 14 shows that the deuteron activation produces less than 10^{-3} dpa for most of the depth and peaks at only about 1 dpa below the activated layer, permitting the conclusion that radiation damage and effects will not affect the results of the measurement.

The depth of activation for the ^{184}Re is about 100 microns, much thicker than that of the α reactions. This allows the benefits of thicker layers, but sacrifices some depth resolution. To regain that resolution however, the activated layer can be compressed by irradiating at an angle to the surface. Figure 15 displays the depth calibration curve for this reaction measured on a target irradiated at an angle of 75° from the normal, compressing the layer by a factor of 4.

The linearity of the depth calibration curve reflects the more uniform density of radioactive tracer associated with this activation. The ratio of actual mass loss to measured mass loss for this profile is plotted in Figure 16, demonstrating much less non-uniformity bias than the α activation. It was hoped that the ^{182}Ta produced in this activation could be used as a second layer to study the surface damage geometry, but the reaction yield is too low to provide usable levels of activity. It may still be possible to use the ^{182}Re since it has a sufficiently high yield, but its short half-life severely limits its useful lifetime.

The deuteron activation produces a number of other intense isotopes, but most of these are very short-lived and decay to negligible levels within days. About 3 weeks after activation the target can be assumed to be a pure ^{184}Re source, which allows simple generation of a reference response function. The ^{182}Re spectrum is sufficiently different from the ^{184}Re spectrum to allow good resolution with the linear least squares approach. The ^{182}Re response function can be generated by subtracting the ^{184}Re response function from the composite spectrum.

The polynomial fit used to interpolate the eroded depth from the depth calibration data yields values with a standard error of 0.2 micrometers, which represents an approximation of the statistical error inherent in this technique. In addition, a systematic error is introduced by using the

thin-slice depth calibration to interpret the data. However, Figure 16 demonstrates that this error is less than a few percent for most of the depth range for the smaller craters and is a significant error only for those craters which punch through the layer. In addition, it must be recognized that these values can be reduced even further if an activated depth of more than 25 micrometers is used. Finally, the use of the ^{182}Re in conjunction with the ^{184}Re may eliminate the uncertainty introduced by the nonuniform geometry of cathode surface damage.

FUTURE APPLICATION OF THE REFINED SLA TECHNIQUE

Although it is important to understand the erosion mechanisms dominating in the microspot emission mode, the unacceptably high erosion rate associated with this emission mechanism mandates exploration of the potentially more benign thermionically emitting cathode. Two independent paths will be followed to investigate this regime of cathode operation--simulation of the hot cathode of a steady state device using a multi-megawatt pulsed MPD thruster and actual time-resolved erosion measurements on a low-power steady state thruster.

PULSED MPD THRUSTER EROSION MEASUREMENTS

A half-scale benchmark thruster[25] similar to that shown in Figure 17 will be used for this series of tests. After obtaining a more reliable set of erosion data from this pulsed device with the bulk cathode surface at about room-temperature to characterize the microspot emission mode, a sequence of testing will be performed with the cathode externally heated prior to the discharge by an inductive coil. This precise control over the bulk surface temperature will allow examining the transition from a cold cathode dominated by microspot emission to an incandescent cathode on which current continuity is satisfied by thermionic emission.

TIME-RESOLVED STEADY STATE THRUSTER EROSION TESTS

The real-time, time resolved erosion measurement technique will be used to study the initial high-erosion start up phase and the less destructive steady-state operation on the coaxial device pictured in Figure 18, which is an MPD-type thruster operated at power levels of up to 30 kW and current levels from 500 to 1000 A for periods of 2 minutes and less[26]. The cathode in this thruster experiences current densities and surface temperatures similar to those expected in high power steady state MPD thrusters. Measurement of the local cathode temperature in conjunction with the mass loss measurements will allow comparison with erosion data taken on the externally heated cathode of the pulsed MPD thruster.

CONCLUSIONS

Preliminary tests of the SLA technique confirm that pulsed thrusters for which bulk cathode temperatures remain below that required for significant thermionic emission are subject to severe erosion associated with the microspot emission mechanism, which renders them useless as practical thrusters. Pulsed devices are useful for simulating the operation of steady state thrusters however, and remain an integral part of the experimental program. Anomalous jumps in the erosion data and the blistered appearance of the activated spot can be attributed to structural radiation damage caused by the high doses of α-particles used in the activation.

The criteria outlined above are designed to address the problem of radiation damage and several deficiencies in the data reduction. The deuteron activation chosen on the basis of these criteria appears capable of providing extremely accurate, non-intrusive measurements of cathode erosion. The deuteron activation parameters and depth calibration curve given above can be used with tungsten surfaces activated in a university or government cyclotron facility or from the commercial activation service offered by the UK Harwell Laboratory in Harwell, England.

Erosion measurements can then be performed with standard radiation measurement equipment similar to that described in the first section of this paper and analyzed on a microcomputer with the gamma spectrum analysis programs noted in the references. The criteria outlined in the second section of the paper can be used to guide the development of an activation scheme appropriate for other materials of interest. Activation, data collection, and interpretation have now reached a sufficient level of sophistication that surface layer activation can become a routine diagnostic technique for studying surface degradation on any material that can be suitably activated.

The planned erosion measurements on the pulsed thruster with the externally heated cathode and the steady state thruster should provide a sound data base for directing and testing erosion modelling efforts. In addition, the time-resolved erosion measurement will demonstrate a new application of surface layer activation that can provide an extremely powerful method of lifetime testing steady state thrusters.

References

1. Polk, J.E., von Jaskowski, W., Kelly, A.J., and Jahn, R.G., "Measurement of MPD Thruster Erosion Using Surface Layer Activation," AIAA Journal of Power and Propulsion, Vol. 3, No. 1, pp. 33-38, 1987.
2. Kelly, A.J., von Jaskowski, W., Polk, J.E., and Jahn, R.G., Advanced Electric Propulsion MPD, AFRPL-TR-86-044, Air Force Rocket Propulsion Laboratory, Edwards Air Force Base, May 1986.
3. Mori, K., Kurikaka, H., and Kuriki, I., Effect of Electrode Configuration on MPD Arcjet Performance, AIAA-84-11, 17th International Electric Propulsion Conference, Tokyo, Japan, July 1984.
4. Buhler, R.D., Auweter-Kurtz, M., and Kurtz, H.L., Plasma Thruster Development, R & D Status Report, AF Contract F 49 620-82-C-0100, Sept. 1983.
5. Wolff, M.J., A High Performance Magnetoplasmadynamic (MPD) Thruster, Mechanical and Aerospace Engineering Dept., Princeton University, Princeton, NJ, Report 1491, Sept. 1980.
6. Marks, L.M., Clark, K.E., von Jaskowski, W.E., and Jahn, R.G., Mpd Thruster Erosion Measurement, AIAA-82-1884, 16th International Electric Propulsion Conference, New Orleans, LA, Nov. 1982.
7. Schrade, H.O., Auweter-Kurtz, M., and Kurtz, H.L., Cathode Erosion Studies on MPD Thrusters, AIAA-85-2007, 18th International Electric Propulsion Conference, Alexandria, VA, Oct. 1985.
8. Rakhovskii, V.I., Experimental Study of the Dynamics of Cathode Spots Development, IEEE Trans. Plasma Sci., PS-4, No. 2, p. 81, 1976.
9. Johnson, C.H., et. Al., "Proton Strength Functions from (p,n) Cross Sections," Phys. Rev., Vol. 109, No. 4, pp. 1243-1254, 1958.
10. Johnson, C.H., et. al., Cross Sections for (p,n) Reactions in Intermediate Weight Nuclei, ORNL-2910, Oak Ridge National Laboratory, Oak Ridge, TN, 1960. Values should be multiplied by 1.43 (private communication).
11. Johnson, C.H., Telephone communication concerning measurements made on thin and thick targets with good repeatability, Physicist, Physics Division, Oak Ridge National Laboratory, Oak Ridge, TN, July 1986.
12. Fano, U., "Penetration of Protons, Alpha Particles, and Mesons," Ann. Rev. Nucl. Sci., Vol. 13, pp. 1-66, 1963.
13. Ziegler, J.F., The Stopping and Ranges of Ions in Matter, 6 volumes, Pergamon Press, 1980.
14. Ahlen, S.P., "Theoretical and Experimental Aspects of the Energy Loss of Relativistic Heavily Ionizing Particles," Rev. Mod. Phys., Vol. 52, No. 1, pp. 121-173, 1980.
15. Quittner, P., Gamma Ray Spectroscopy, Halsted Press, 1972.
16. Schonfeld, E., et al., "Determination of Nuclide Concentrations in Solutions Containing Low Levels of Radioactivity by Least Squares Resolution of the Gamma-Ray Spectra," Nuclear Instruments and Methods, Vol. 45, pp. 1-21, 1966.
17. Schonfeld, E., ALPHA-M, An Improved Computer Program for Determining Radioisotope Concentrations by Least-Squares Resolution of the Gamma-Ray Spectra, ORNL-3975, Oak Ridge National Laboratory, Oak Ridge, TN, Sept. 1966.
18. Polk, J.E., Kelly, A.J., and Jahn, R.G., Advanced Electric Propulsion MPD, Technical Progress Report 87, AF Contract F 04611-85-C-0021, Nov., 1986.
19. Mansur, L.K., "Mechanisms and Kinetics of Radiation Effects in Metals and Alloys," in Kinetics of Nonhomogeneous Processes, ed. by Freeman, G.R., Wiley, 1987.
20. Kaminsky, M., Atomic and Ionic Impact Phenomena On Metal Surfaces, Springer-Verlag, 1965.
21. Chadderton, L.T., Radiation Damage in Crystals, Wiley, 1965.

22. Lindhard, J., Scharff, M., and Schiott, H.E., Mat. Fys. Medd. Dan. Vid. Selsk, Vol. 33, No. 14, 1963.
23. Conlon, T.W., Telephone conversation concerning radiation damage in surface layer activation, Physicist. UK Harwell Lab, AERE, England, Nov., 1986.
24. Asher, J., and Conlon, T.W., "Double Layer Activation for the Detection of Non-uniform Wear or Corrosion," Nuclear Instruments and Methods, Vol. 179, pp. 201-205, 1981.
25. Kaplan, D.I., and Jahn, R.G., Performance Characteristics of Geometrically-Scaled Magnetoplasmadynamic (MPD) Thrusters, Mechanical and Aerospace Engineering Dept., Princeton University, Princeton, NJ, Report 1632-T, 1983.
26. Myers, R., Kelly, A.J., and Jahn, R.G., Electrothermal-Electromagnetic Hybrid Thruster Research, AIAA Paper 87-1018, 19th International Electric Propulsion Conference, Colorado Springs, CO, May, 1987.

Table 1: Activation Parameters

Parameter	Target W (cathode)	Target C$_{60}$ (carbon)	Target BN (backplate)
Radioisotope	^{185}Os	^{63}Zn	^{7}Be
Beam Particle	[illegible]	[illegible]	[illegible]
Beam Energy (MeV)	[illegible]	[illegible]	2.4
Total Charge on Target (mC)	[illegible]	[illegible]	[illegible]
Activity (μCi)	[illegible]	[illegible]	[illegible]
Production Yield (μCi / mC)	[illegible]	[illegible]	[illegible]

Table 2: [illegible]

Range (discharges)	Erosion Rate (μg / cm^2 shot)	Range (10^3 C)	Erosion Rate (μg / cm^2 C)
629-1301	[illegible]	[illegible]	[illegible]
2103-4023	[illegible]	[illegible]	[illegible]
5426-8653	[illegible]	[illegible]	[illegible]
8785-9988	[illegible]	[illegible]	[illegible]
10780-13883	[illegible]	[illegible]	[illegible]

Table 3: Comparison of Tungsten Activations

Beam	Beam Energy (MeV)	Reactions	Yield (μCi/C)	Activated Area* (cm^2)	Axial Resolution** (cm)	Activated Depth† (μm)	Half-life (days)	Major γ Lines (keV)
α	23	$^{182}W(\alpha,n)^{185}Os$ $^{183}W(\alpha,2n)^{185}Os$ $^{184}W(\alpha,3n)^{185}Os$ $^{186}W(\alpha,5n)^{185}Os$	50	6.25	2.93	26	93.6	646
d	15	$^{182}W(d,\gamma)^{184}Re$ $^{183}W(d,n)^{184}Re$ $^{184}W(d,2n)^{184}Re$ $^{186}W(d,4n)^{184}Re$	7000	0.05	0.02	100	38.0	792 895 903
		$^{182}W(d,2p)^{182}Ta$ $^{184}W(d,\alpha)^{182}Ta$	40	8.75	3.50	70	115.0	1121, 1189 1221, 1231
		$^{182}W(d,2n)^{182}Re$ $^{183}W(d,3n)^{182}Re$ $^{184}W(d,4n)^{182}Re$	15,000	0.02	0.01	——‡	2.67	169, 229 256, 351 1076, 1121

* Area for 1 μCi activity at a dose of 10^{16} cm^{-2}

** Axial length of circumferential activated strip, assuming area from column 6 and an attenuation of 32%

† For beam normal to the surface

‡ Not yet measured

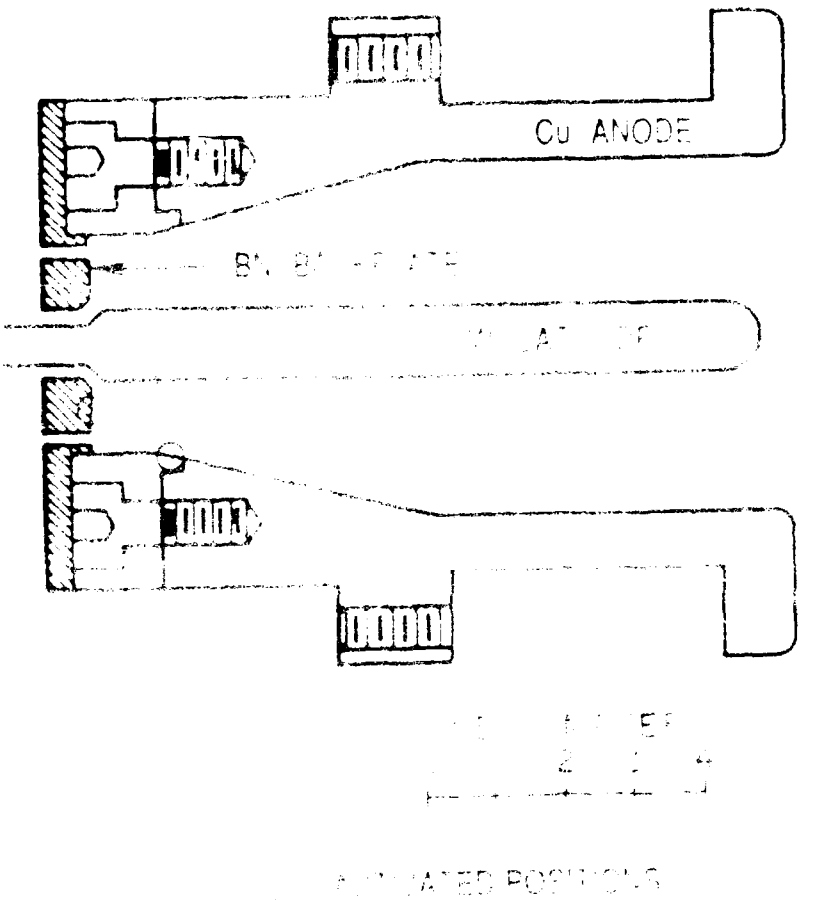

Figure 1. Hall [illegible] thruster

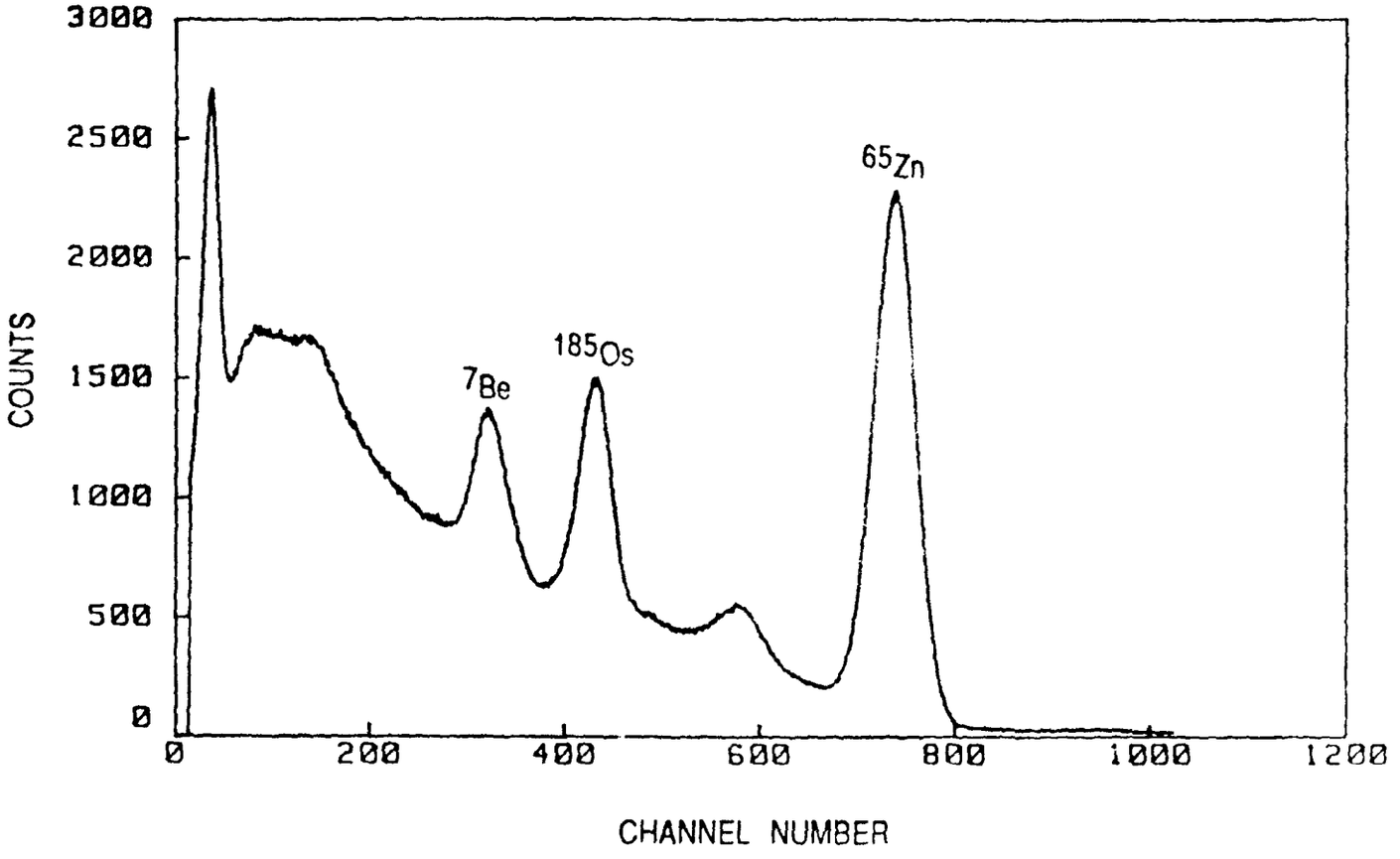

Figure 2: Composite gamma-ray spectrum.

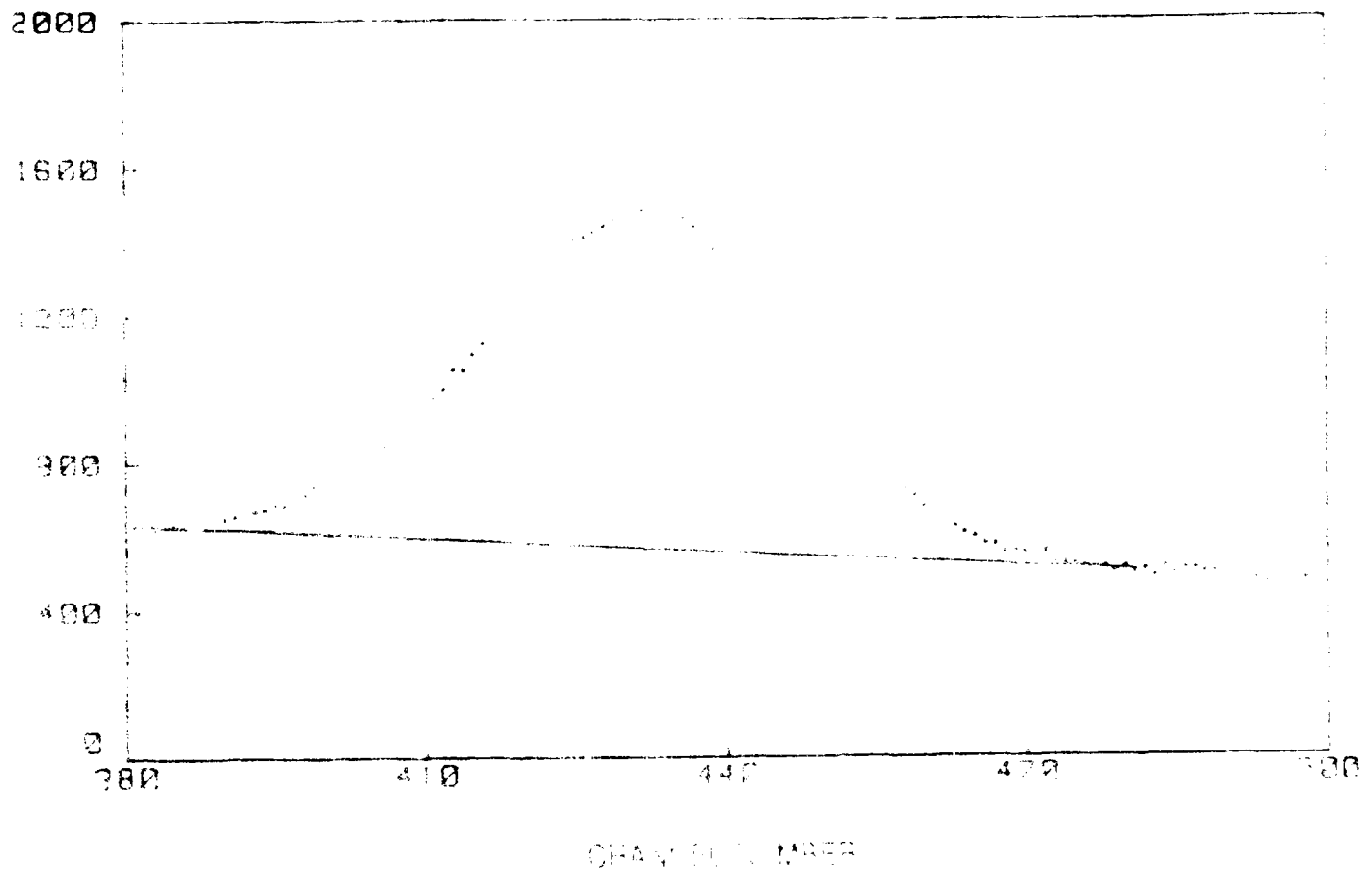

Figure 3: [illegible] area [illegible] by linear background [illegible]

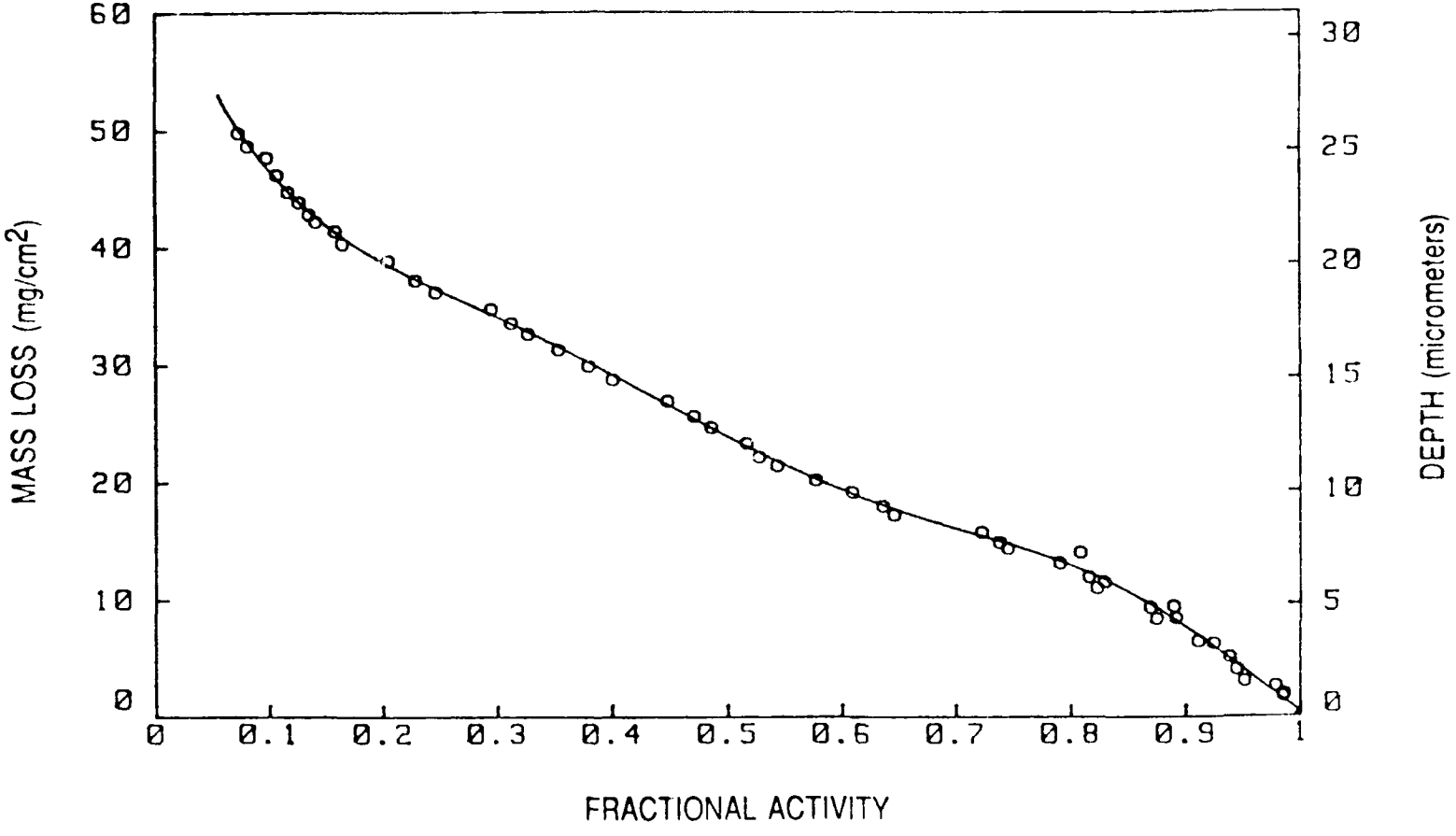

Figure 4: Depth calibration for tungsten activated with 23 MeV alpha particles normal to the surface.

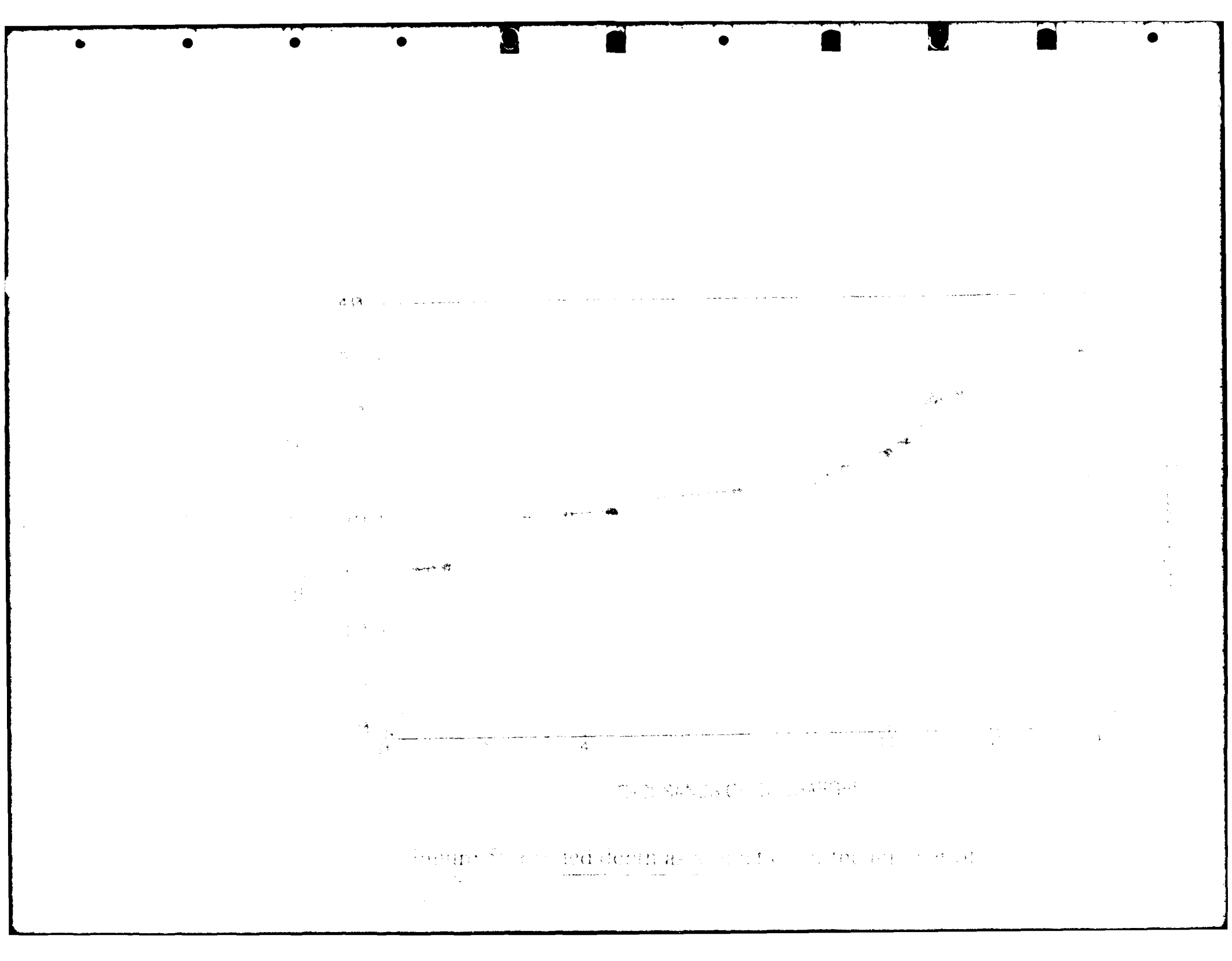

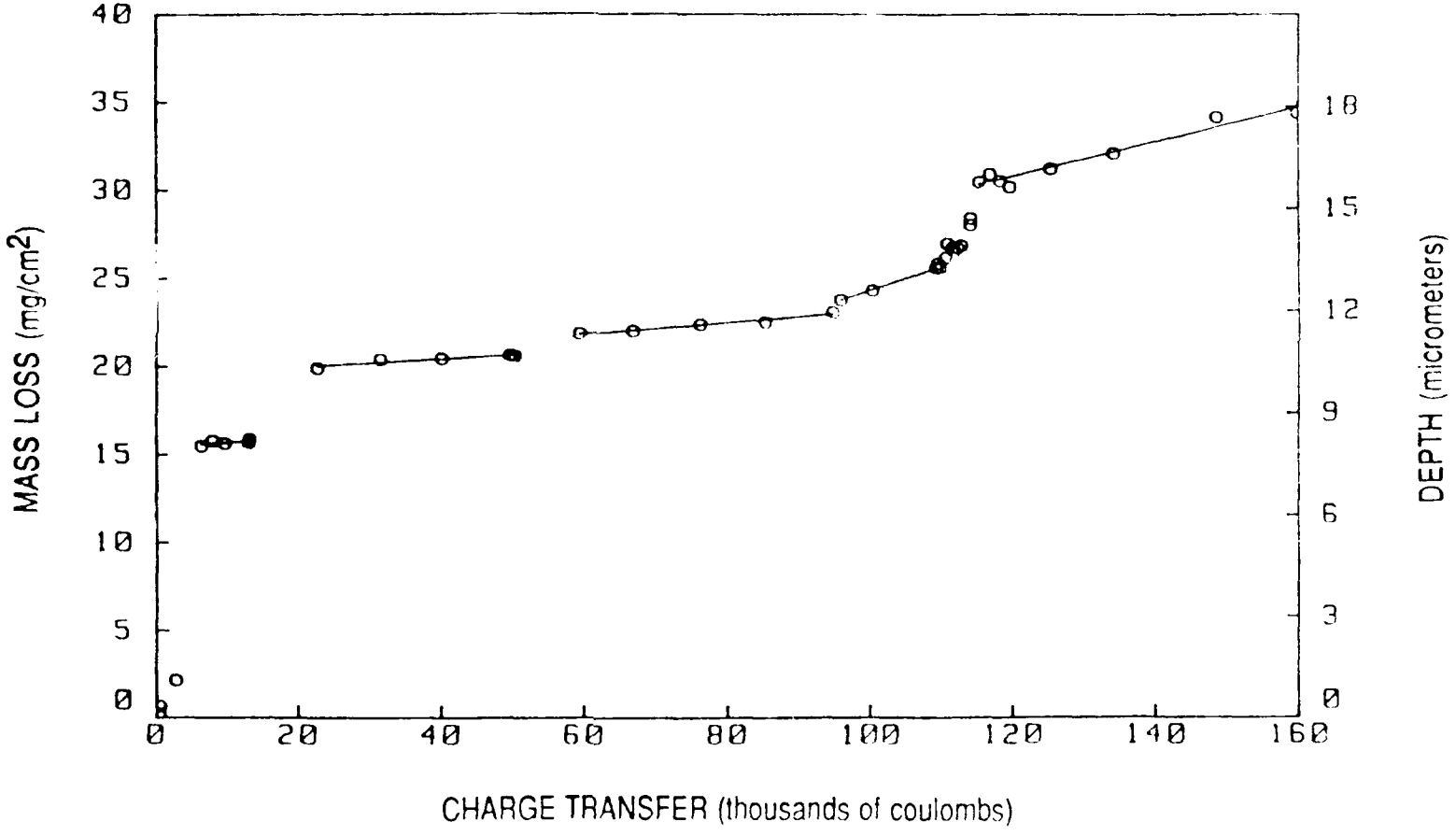

Figure 6: Eroded depth as a function of the total charge transfer.

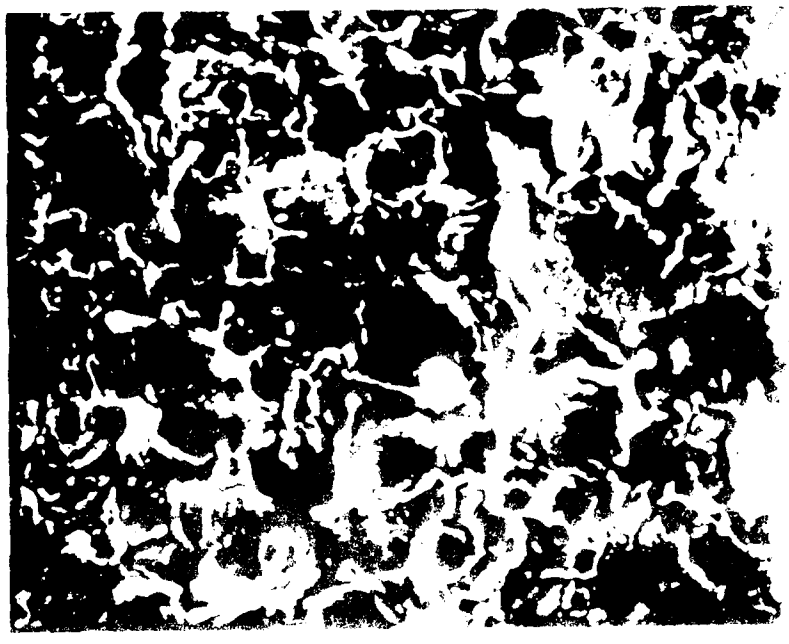

magnification

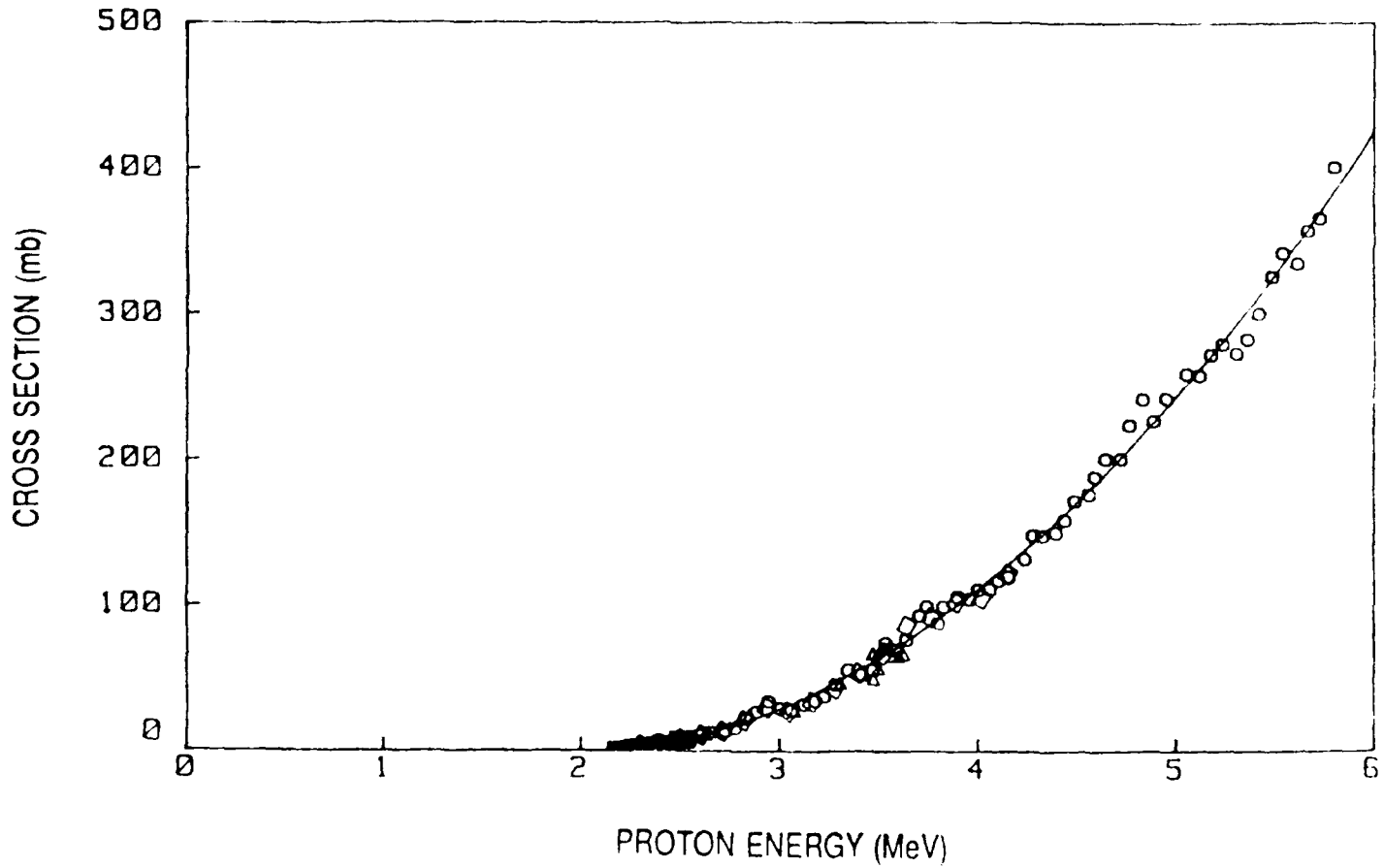

Figure 8: Cross-section data for the $^{65}Cu(p,n)^{65}Zn$ reaction.

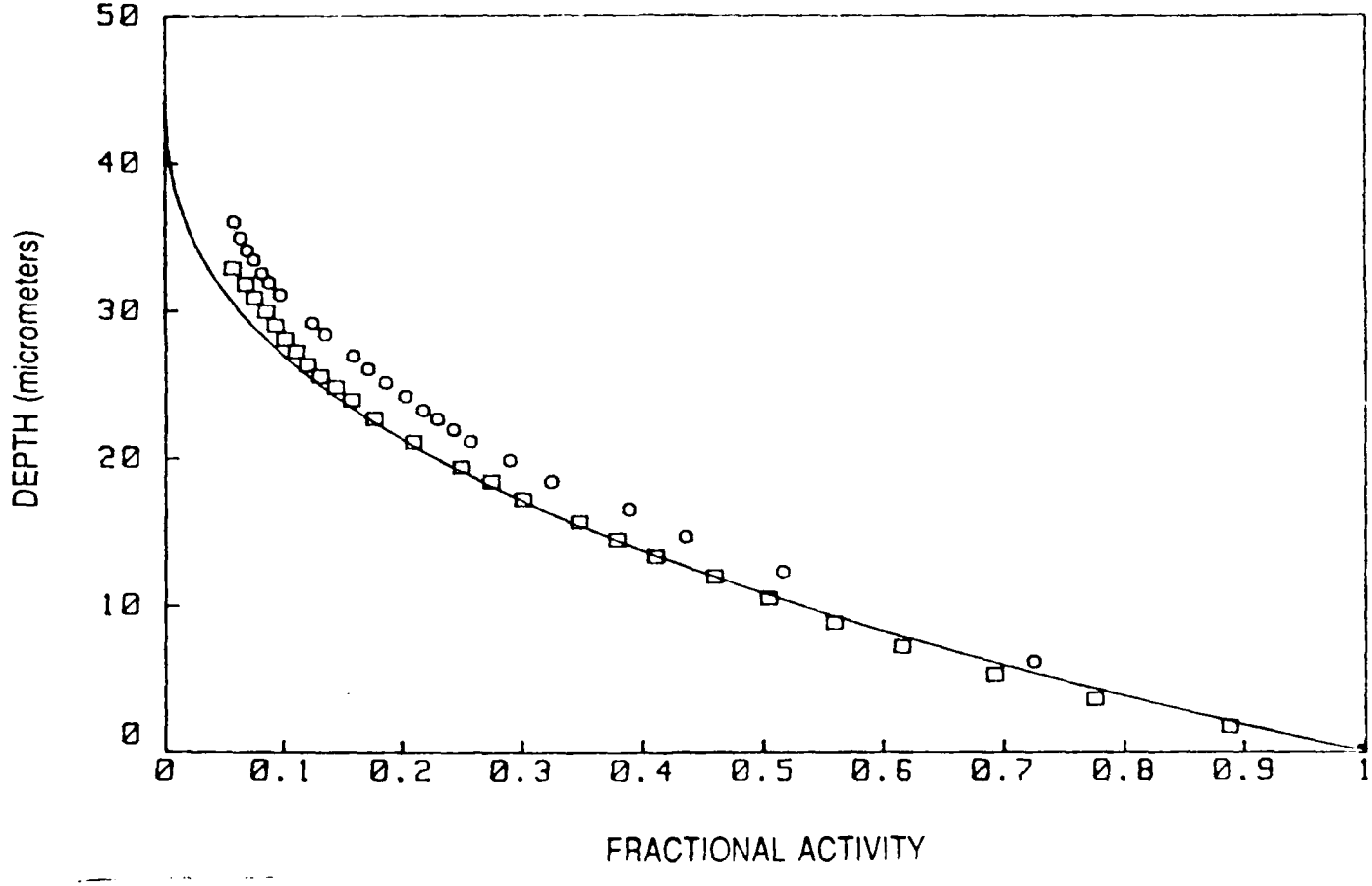

Figure 10: Comparison of calculated (–) and measured (o, □) depth calibration curves for 4.51 MeV protons normal to copper surface.

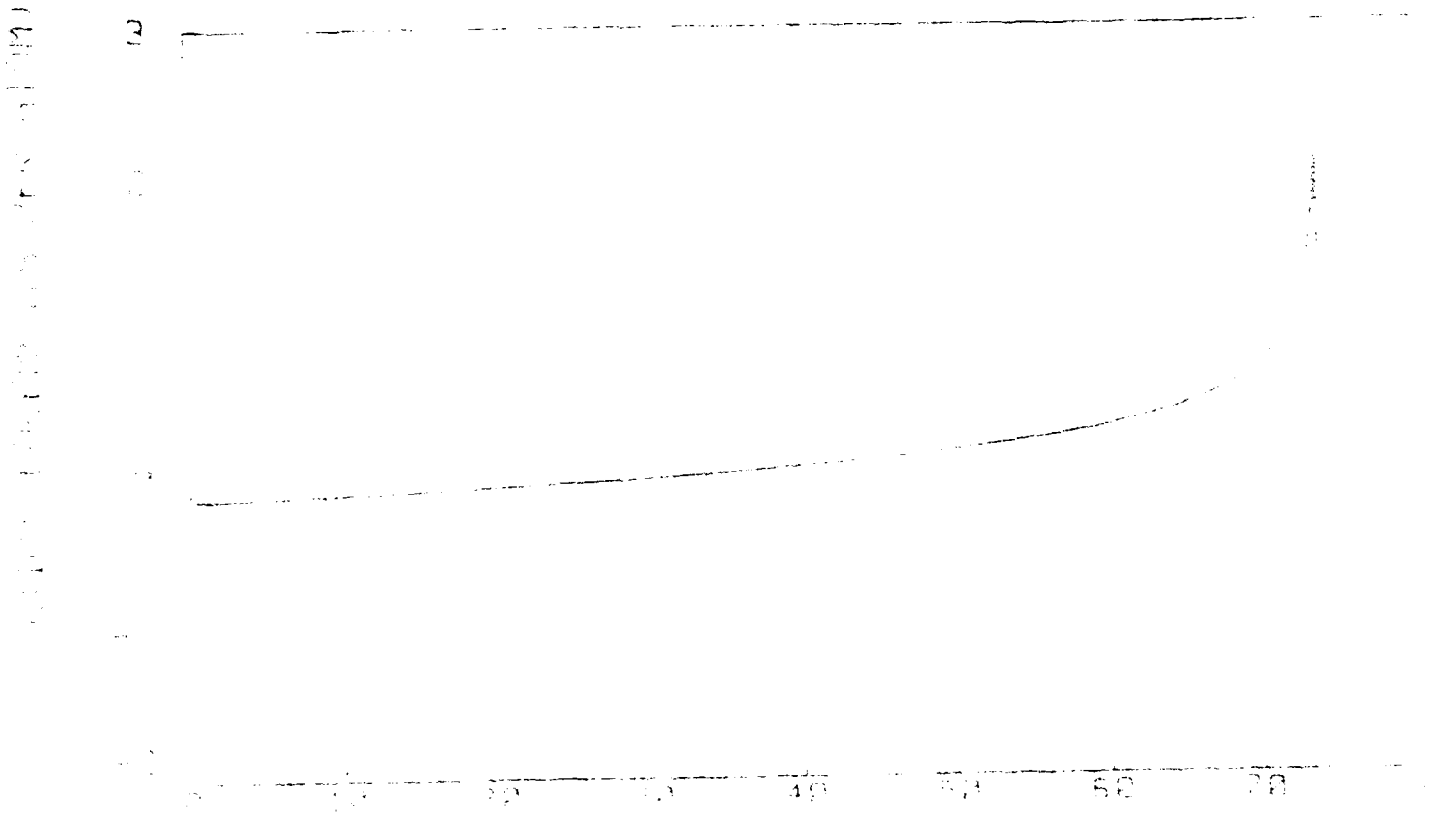

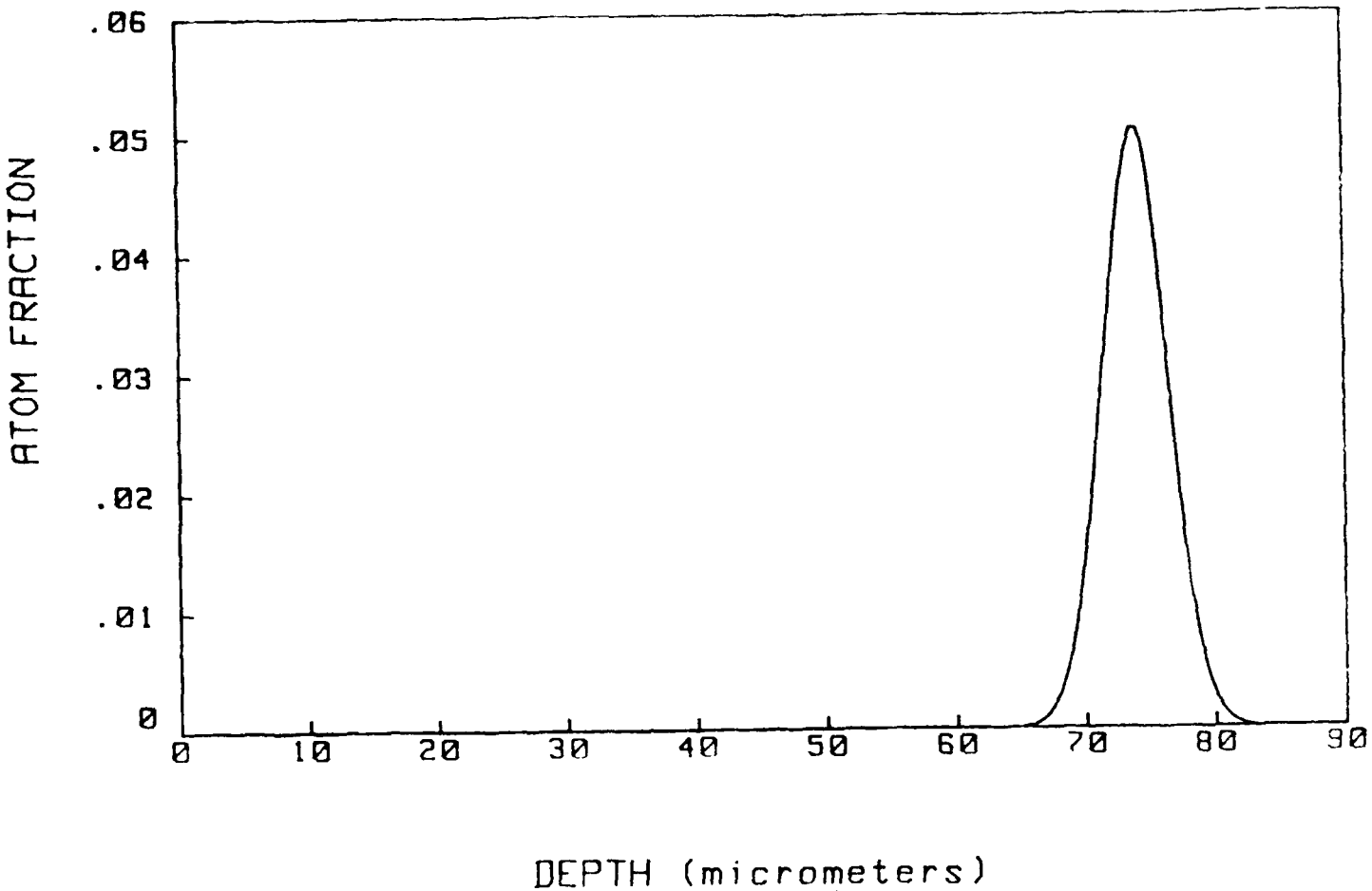

Figure 12: Profile of implanted He in tungsten.

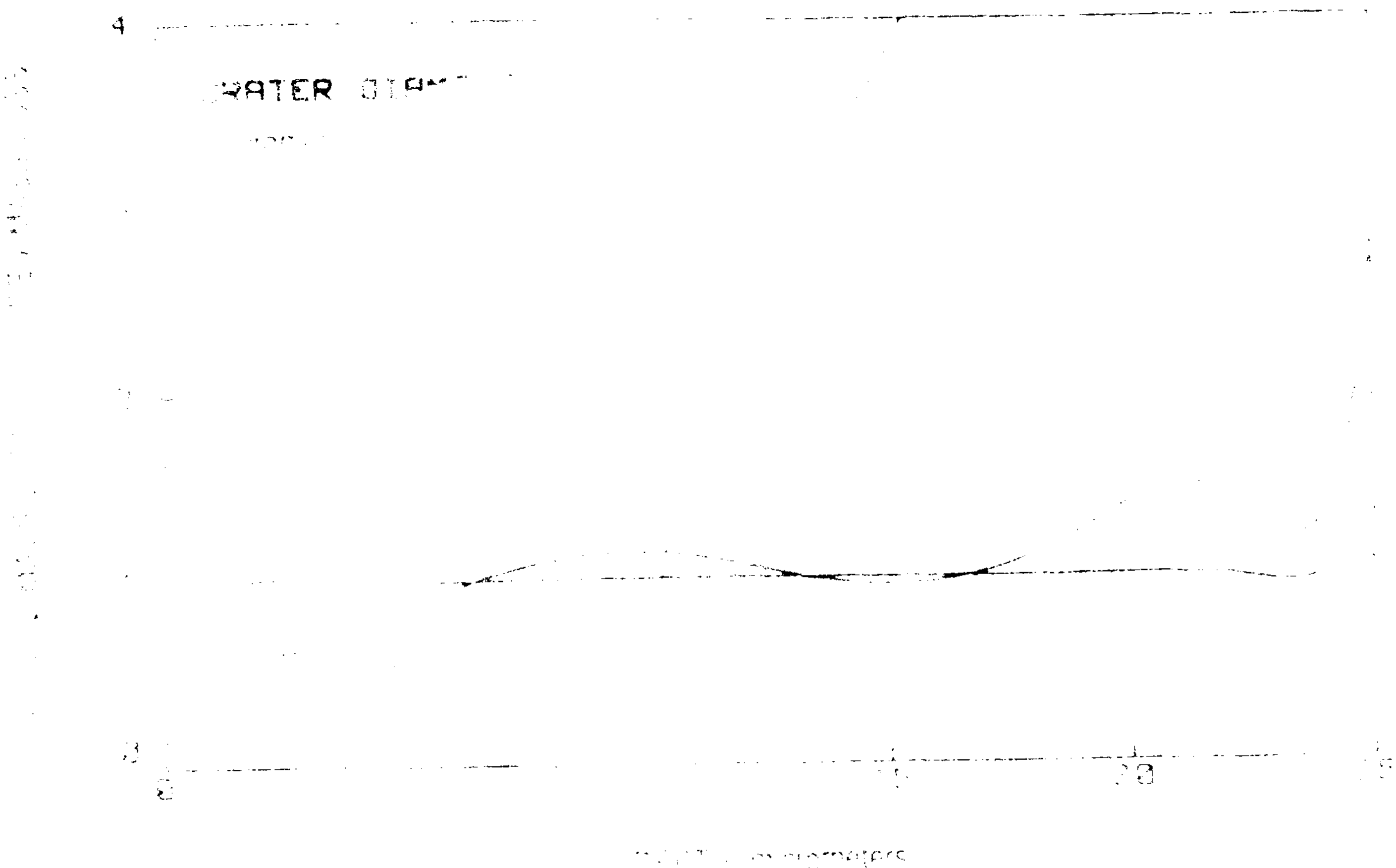

Figure [illegible] depth calibration [illegible]
[illegible] for [illegible] MeV [illegible]

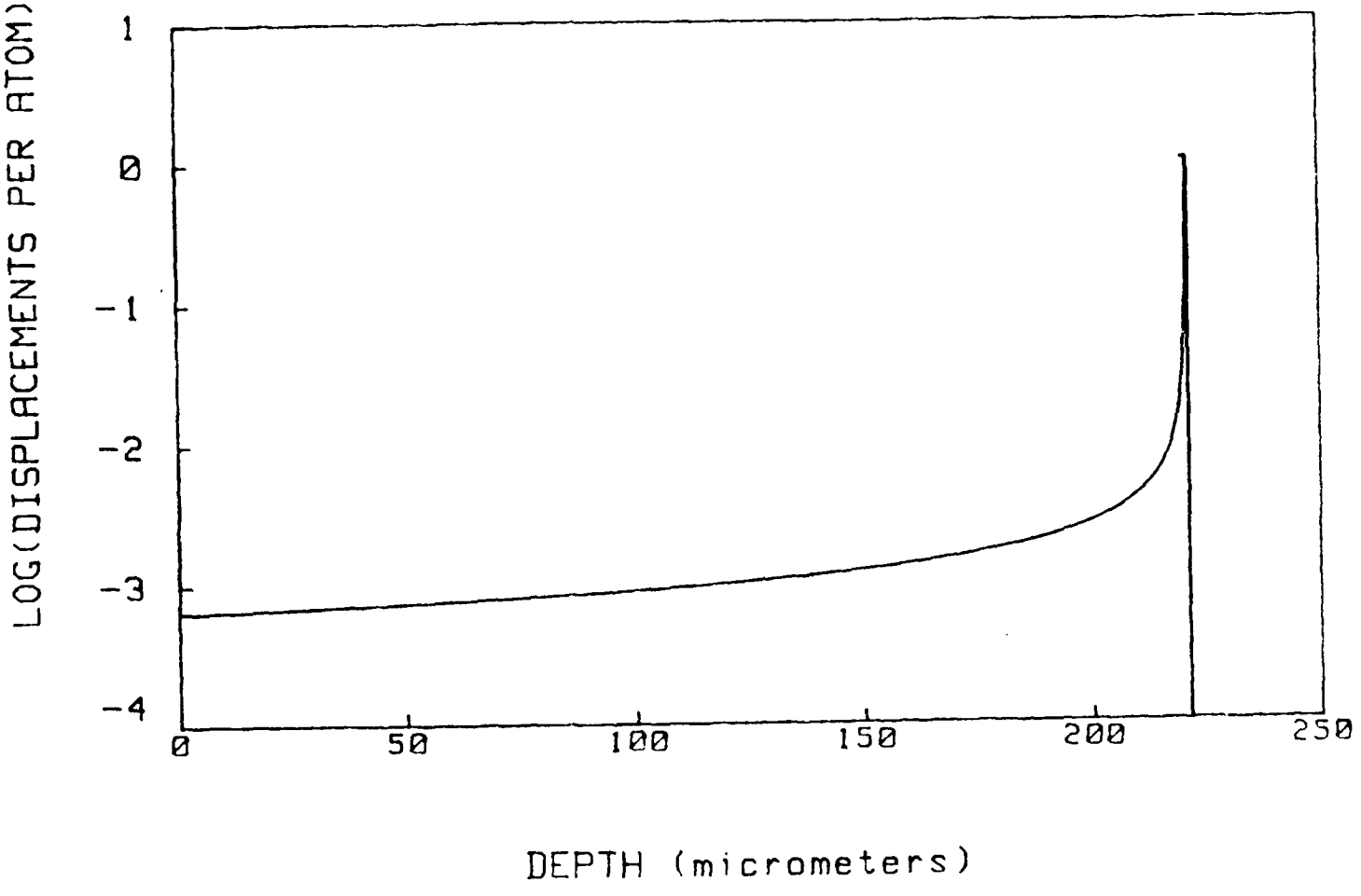

Figure 14: Damage profile for tungsten activated with 15 MeV deuterons normal to the surface.

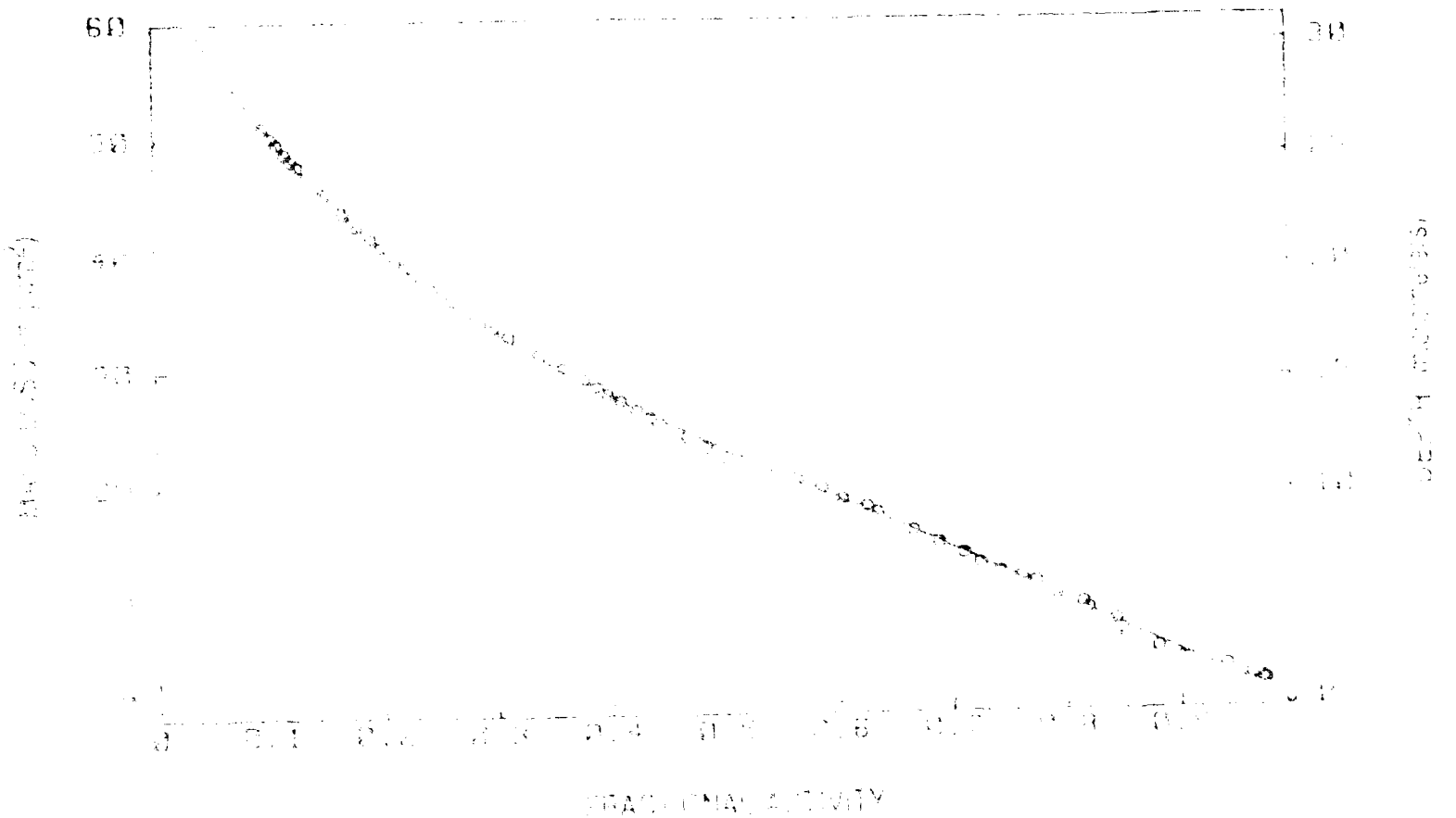
60
30

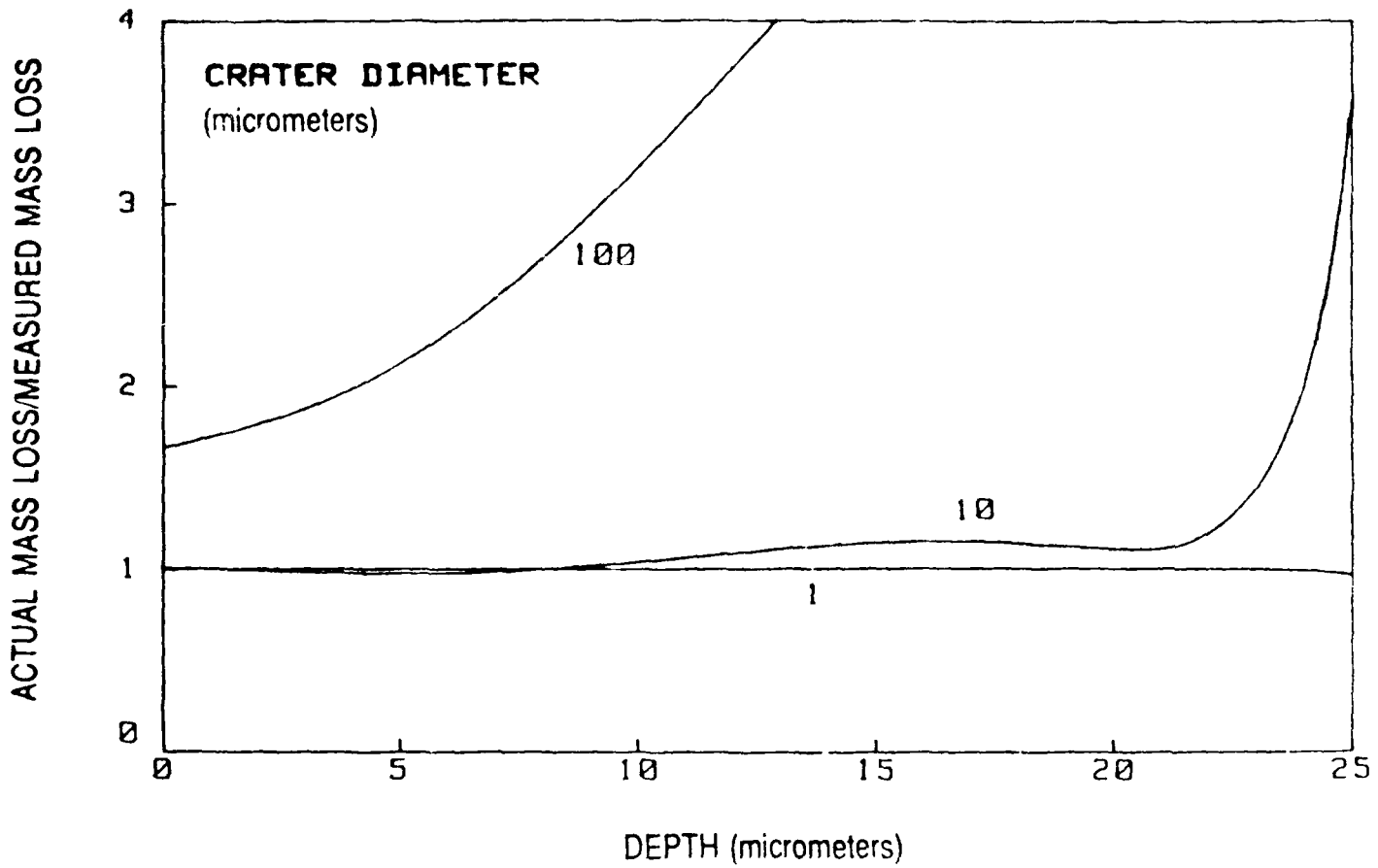

Figure 16: Non-uniform erosion bias for tungsten deuteron activation.

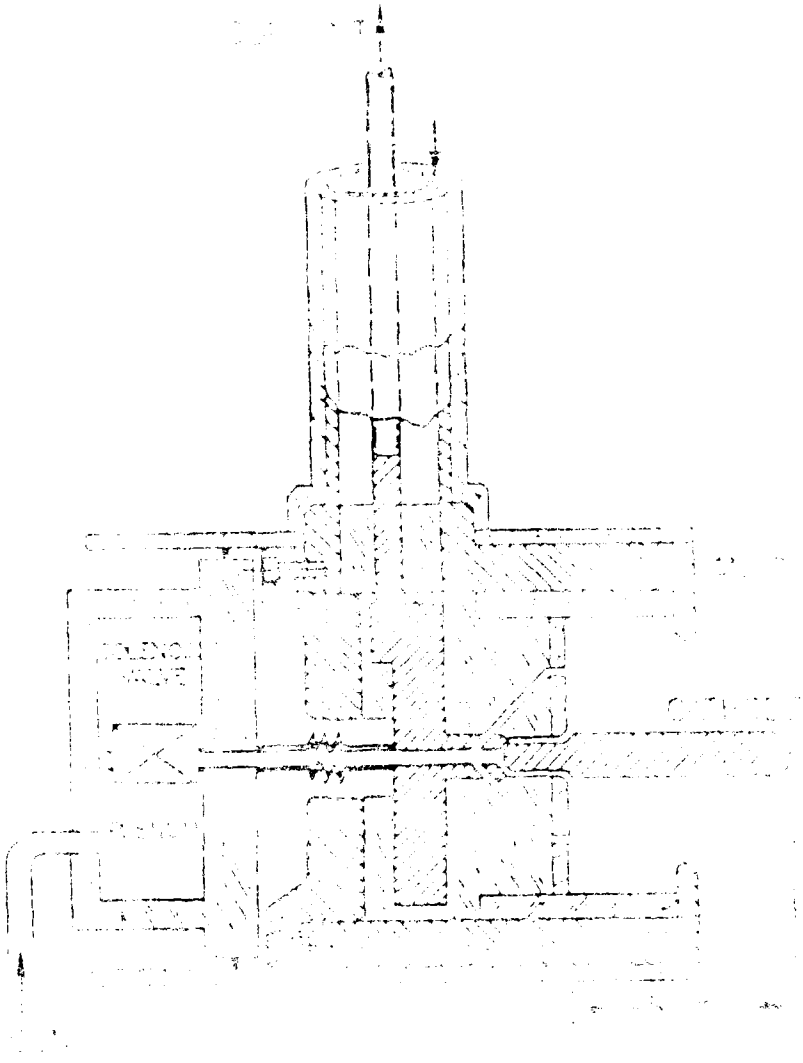

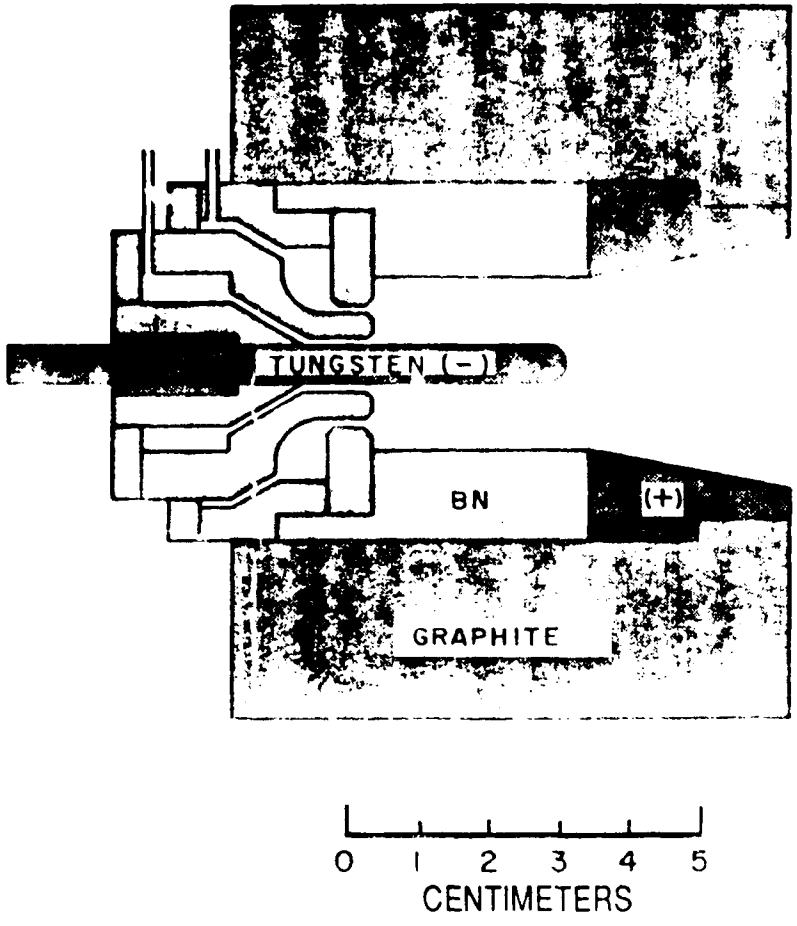

Figure 18. Low power, steady-state MPD thruster.